"Dial-In" Emission from Unique Flexible Material with Polarization Tuneable Spectral Intensity

Article *in* Chemistry - A European Journal · August 2019

DOI: 10.1002/chem.201902333

8 authors, including:

Rajan Kumar
The Assam Royal Global University
15 PUBLICATIONS **68** CITATIONS
SEE PROFILE

Subir Kumar Ray
University of Toronto
23 PUBLICATIONS **126** CITATIONS
SEE PROFILE

Saikat Mukherjee
Indian Institute of Science Education and Research Kolkata
18 PUBLICATIONS **112** CITATIONS
SEE PROFILE

Sudipta Saha
Indian Institute of Science Education and Research Kolkata
17 PUBLICATIONS **106** CITATIONS
SEE PROFILE

ChemPubSoc Europe

DOI: 10.1002/chem.201902333

CHEMISTRY A European Journal Full Paper

Photoluminescent Materials

"Dial-In" Emission from a Unique Flexible Material with Polarization Tuneable Spectral Intensity

Rajan Kumar,[a] Subir Kumar Ray,[b] Saikat Mukherjee,[a] Sudipta Saha,[b] Arijit Bag,[c] Pradip Kr. Ghorai,[c] Nirmalya Ghosh,[b] and Raja Shunmugam*[a]

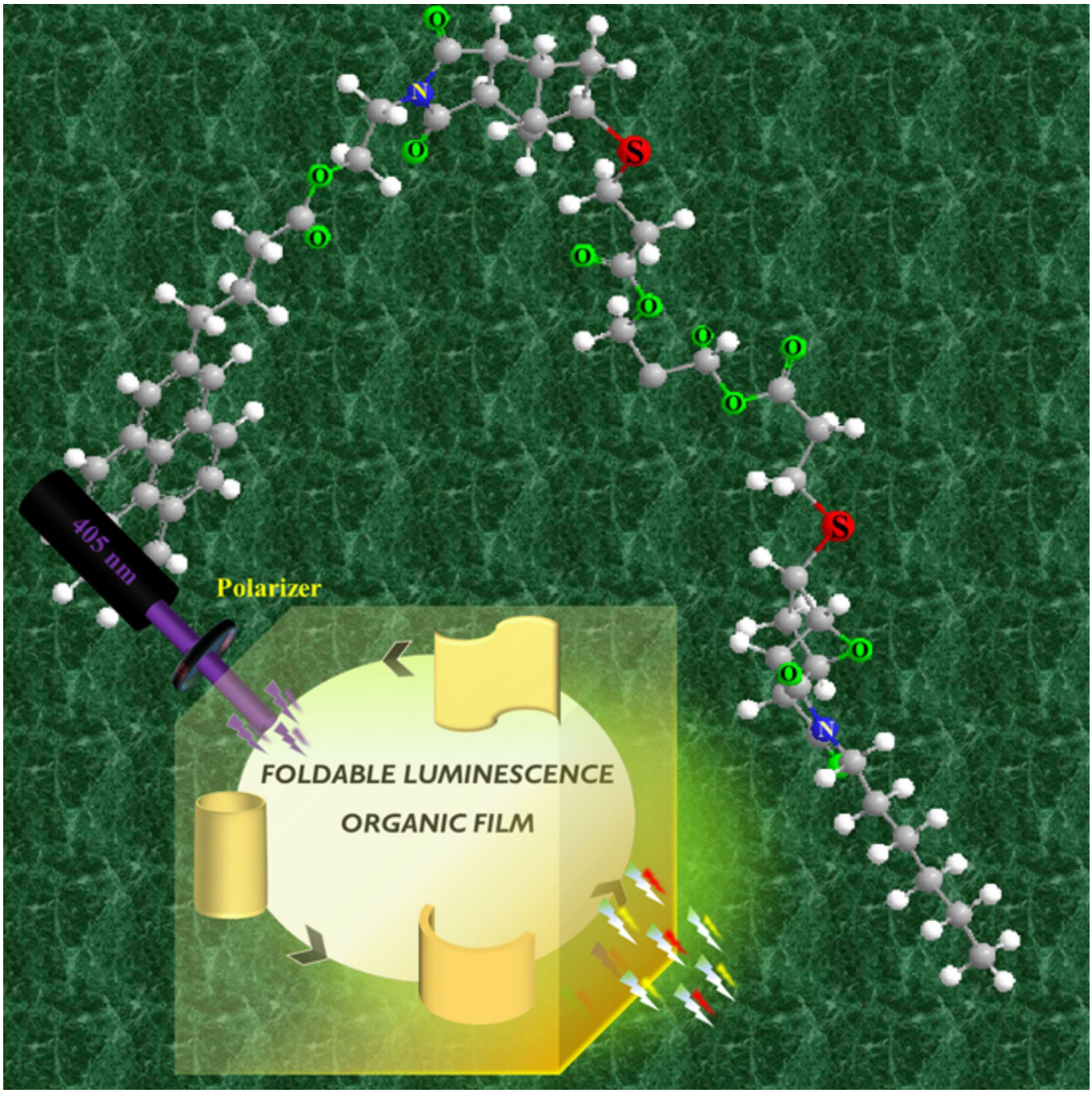

Abstract: The development of organic photoluminescent materials, which show promising roles as catalysts, sensors, organic light-emitting diodes, logic gates, etc., is a major demand and challenge for the global scientific community. In this context, a photoclick polymerization method is adopted for the growth of a unique photoluminescent three-dimensional (3D) polymer film, E, as a model system that shows emission tunability over the range 350–650 nm against the excitation range 295–425 nm. The DFT analysis of energy calculations and π-stacking supports the spectroscopic observations for the material exhibiting a broad range of emission owing to newly formed chromophoric units within the film. Full polarization spectroscopic Mueller matrix studies were employed to extract and quantify the molecular orientational order of both the ground (excitation) and excited (emission) state anisotropies through a set of newly defined parameters, namely the fluorescence diattenuation and fluorescence polarizance. The information contained in the recorded fluorescence Mueller matrix of the organic polymer material provided a useful way to control the spectral intensity of emission by using pre- and post-selection of polarization states. The observation was based on the assumption that the longer lifetime of the excited dipolar orientation is attributed to the compactness of the film.

Introduction

A recent survey highlighted the rapid global development of photoluminescent molecules. Such luminescent molecules are either comprised of inorganic constituents or organic–inorganic hybrid constituents.[1] Both inorganic and hybrid organometallic luminescent material have come to dominate the field, although some limitations remain. New approaches have invoked the use of modified organic–inorganic hybrids, but their prolonged efficiency remains one of the major concerns. Therefore, with the focus on such drawbacks, the field is slowly switching to the development of luminescent organic materials. Extensive research has been done on conjugated fluorophore based diodes, whereas reports on intact π-stacked 3D photoluminescent polymer films is limited.[2–11] After thorough examination of literature examples, we believe that with modification of the existing systems would provide superior materials with excellent features related to sensing, organic light-emitting diodes (OLEDs), catalysis, etc. First, we wanted to adopt a simple and facile synthetic approach. Secondly, this approach should give an intact π-stacked polymer film where the chromophore constituents introduced should have a static phase. The additional features that we expected to mould and incorporate within the modelled luminescent macromolecular film are flexibility, stability, insolubility, easy handling, among others. Considering all these points, herein, we report the design, synthesis, and demonstration of a newly developed photoluminescent polymer material. We have utilized the thiol–alkene photoclick polymerization reaction to grow such polymer material.[13–15] The polymerization is a two-plane polymerization process, which gives rise to three dimensional (3D) polymer material in the form of a film. This polymer film grown by the proposed photopolymerization technique is likely to be stable. Our proposed photopolymerization method has been highlighted in Scheme 2a.

Further, we have explored the fluorescence Mueller matrix (MM) spectroscopy technique for probing the polarization anisotropies of the film arising owing to its crosslinked organization. The fluorescence polarization spectroscopy has shown considerable promise for characterization of different chemical, biological, and complex physical systems. Traditionally, fluorescence polarization anisotropy is quantified by the anisotropy parameter $r=(I_{\parallel}-I_{\perp})/(I_{\parallel}+2I_{\perp})$ in which $I_{\parallel}$ and $I_{\perp}$ are, respectively, the measured fluorescent intensities parallel to and perpendicular to the excitation linear polarization.[16] The anisotropy parameter (r) contains information about the inherent depolarization associated with the fluorescence emission. Depolarization in the case of fluorescence is caused by the random orientation of fluorophores, radiationless energy transfer among fluorophores, and extrinsic causes like multiple scattering effects, etc. Thus, the resulting anisotropy parameter contains lumped information about all the contributing polarizing and depolarizing effects associated with the fluorescence scattering process. In addition to the intrinsic and extrinsic causes of depolarization, it is useful to capture and quantify exclusive information of the molecular orientation and organization of the fluorescent molecules. For this purpose, we have employed Mueller matrix (transfer function of an optical system) measurements for quantification of organizational anisotropies of

[a] *R. Kumar, Dr. S. Mukherjee, Prof. Dr. R. Shunmugam*
Polymer Research Centre (PRC), Centre for Advanced Functional Materials (CAFM), Department of Chemical Sciences
Indian Institute of Science Education and Research Kolkata (IISER K)
Mohanpur, West Bengal, 741 246 (India)
E-mail: sraja@iiserkol.ac.in

[b] *S. K. Ray, S. Saha, Prof. Dr. N. Ghosh*
Department of Physical Sciences, Indian Institute of Science Education and Research Kolkata (IISER K), Mohanpur, West Bengal 741 246 (India)

[c] *Dr. A. Bag, Prof. Dr. P. K. Ghorai*
Department of Chemical Sciences, Indian Institute of Science Education and Research Kolkata (IISER K), Mohanpur, West Bengal 741 246 (India)

Supporting information and the ORCID identification number(s) for the author(s) of this article can be found under: https://doi.org/10.1002/chem.201902333. The Supporting Information contains the synthetic scheme for polymer D, synthetic procedures for A, A′, B, C, polymer D, and E, ^{1}H NMR and ^{13}C NMR spectra for A, A′, B, and C, ^{1}H NMR spectra for polymers D and E, comparative ^{1}H NMR spectra for polymers D and E, ESI-MS for the synthesized monomers A, A′, B, and C, TGA analysis for polymers D and E, ATR-FTIR curves of 4SH, monomer B, monomer C, polymers D and E, comparative UV analysis of 4S, monomer B, and monomer C, mechanism of formation of pyrene crosslinked polymer E, HOMO–LUMO energy state calculations, Muller matrix analysis, FE SEM, EDX, and mapping analysis for polymers D and E.

both the excitation and emission states of the molecule. These anisotropies manifest themselves as differential excitation of fluorescence with orthogonal polarization (both linear and circular) and differential emission of fluorescence for orthogonal polarization (both linear and circular). These anisotropies are quantified through the various elements of the recorded fluorescence Mueller matrix. Note that the Mueller matrix polarimetry is usually used and is well-explored for elastic scattering processes like reflection, refraction, etc.[17,18] Recent theoretical and experimental studies by our group and others have extended Muller matrix measurements to inelastic scattering processes like fluorescence.[19,20] The inverse analysis of the fluorescence Mueller matrix has enabled us to quantify the excitation and emission state anisotropies through a set of newly defined polarimetry parameters, namely, the fluorescence diattenuation (differential excitation of fluorescence) and fluorescence polarizance (differential emission of fluorescence).[21] These are then used to quantify the molecular orientational order of the organic polymer domain, and finally, the polarization anisotropies of fluorescence emission showed useful application involving polarization based tuning of spectral intensity.

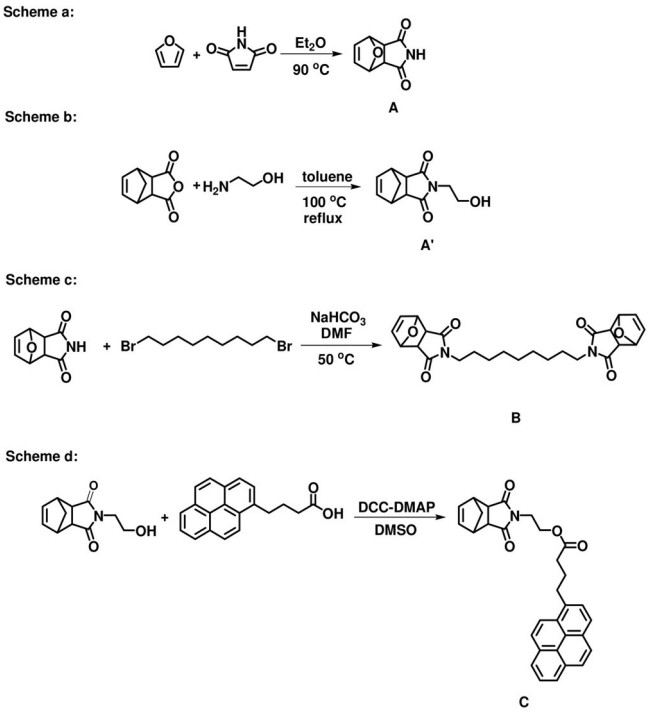

Scheme 1. a–d) Synthesis of compounds A, A′, B, and C.

Results and Discussions

Photoluminescent materials are a typical example for future utilization in a scientific and global society. With this in mind, there is a need to upgrade the efficiency in terms of tunability and mechanical properties. We first undertook the photopolymerization of the synthesized monomers B and C (Scheme 1), with the commercial monomer pentaerythritoltetrakis (3-mercaptopropionate) tetrathiol (4SH) to grow the photoluminescent 3D polymer film E (abbreviated as polymer E) as shown in Scheme 2a. To check the film formation, the non-luminescent 3D polymer film D (abbreviated as polymer D) was also synthesized. The synthetic scheme for polymer D is shown in the Supporting Information. The synthetic routes for the monomers required for the growth of polymer E are shown in Scheme 1. All the monomers were well characterized by using NMR spectroscopy, mass spectrometry, and FTIR-ATR (attenuated total reflection) spectroscopy techniques (Figures S1–S8, S13–S17, in the Supporting Information). The formation of polymers D and E was confirmed by NMR spectroscopy (Figures S9, S10, in the Supporting Information) and FTIR-ATR spectroscopy techniques (Figure S18, in the Supporting Information). The comparative ^{1}H NMR spectra confirmed the propagation of polymerization and product formation (Figures S11, S12, in the Supporting Information). Comparative FTIR-ATR spectra supported these results well: the thiol (-SH) signal at 2535 cm^{-1} disappeared for the polymers (Figure S18, in the Supporting Information). This confirmed that thiolation had occurred during the photopolymerization process. The thermogravimetric analysis (TGA) curves for both the polymers D and E confirmed their thermal stability (Figure S20, in the Supporting Information). The morphology for the materials was observed using field emission scanning electron microscopy (FE SEM; Figure S22, in the Supporting Information). The energy dispersive X-ray (EDX) and mapping for the respective polymers was also analysed (Figures S23 and 24, in the Supporting Information). These observations supported the presence of carbon, oxygen, nitrogen, and sulfur. Comparative UV spectroscopy for the monomers was recorded as shown in Figure S19 (in the Supporting Information). This confirmed only monomer C showing absorbance up to 350 nm. The physical observation under ultraviolet (UV) light reveals polymer E containing chromophore C emits white light with excitation at a wavelength of 365 nm (Scheme 2c). The basic principle that governs photoluminescence in devices is a combination of charge injection (CI) and charge recombination (CR) that is, back electron transfer (BET).[22] Based on this, in-depth analysis has been undertaken to check the tunability of polymer E. During the growth process of pyrene-based polymer E, the reaction mixture was allowed to stabilize. The reorientation and interlocking owing to π-stacking occurred within the reaction mixture. The polymer E film thus grown was flexible, transparent, and compressible (Scheme 2b). The probable mechanism to formation of polymer E is shown in Figure S21 (in the Supporting Information).

The proposed mechanism has been highlighted for a single thiol–alkene moiety. The thiol radical (-S$^{\bullet}$) generated in step 1 reduces the alkenes B and C in substages. The free radical crosslinking proceeds repeatedly unless the saturation and the randomness of the monomers ceases. The polymer E with white light emission was analysed by using solid-state ultraviolet (UV) and fluorescence spectroscopy. The solid-state UV and fluorescence spectroscopic analysis supported our physical observations. The UV curve shows the polymer E covers the range 250–600 nm, whereas the emission spectrum covered the range for red, green, and blue (RGB; Figure 1a, b). To value

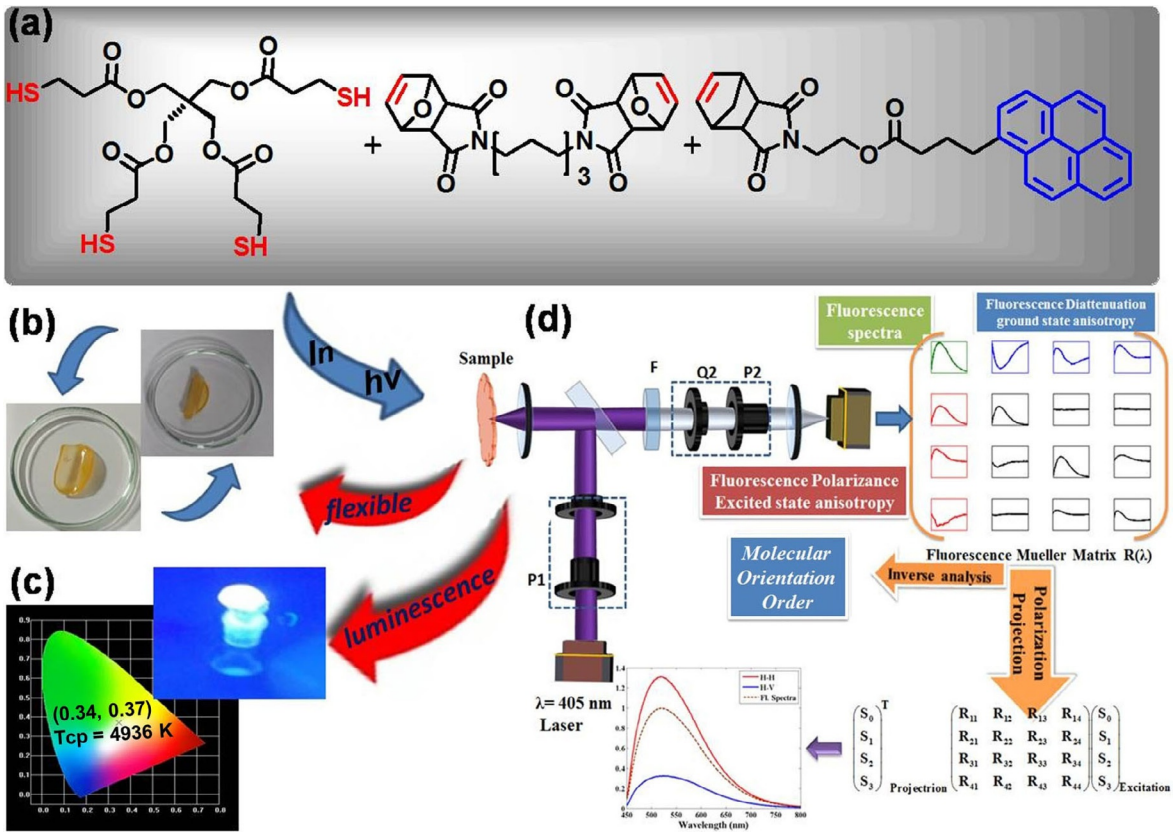

Scheme 2. a) Synthesis of polymer E (sample). b) Flexibility and c) luminescence of polymer E. d) Schematic of the experimental spectroscopic fluorescence Mueller matrix setup. F: long-pass filter; P1 and P2: linear polarizers; Q1 and Q2: achromatic quarter-wave retarders. P1 and Q1 form the polarization state generator (PSG) unit. P2 and Q2 form the polarization state analyser (PSA) unit. The inverse analysis of the recorded fluorescence Muller matrix gives anisotropies of the ground and excited molecular states, namely fluorescence diattenuation and polarizance, respectively. The 4×4 fluorescence spectroscopic Mueller matrix R (λ = 450–800 nm) recorded from the gel sample. The first element (R_{11}) represents the polarization independent fluorescence spectra. The other three elements in the first row (blue) represent the excitation anisotropy related to the ground molecular state whereas the three elements in the first column (red) represent the emission anisotropy related to the excited molecular state.

the white colour and emissive properties, Commission International de l'Eclairage (CIE) chromaticity coordinates (x,y) were calculated.[23–25] The colour coordinates were 0.34 and 0.37, falling in range of white light CIE coordinates (x = 0.33, y = 0.33). The correlated colour temperature, T_{cp} for the polymer E is 4936 K. The T_{cp} value is around that of a light source of a cool compact fluorescent lamp (CFL).

Further to check the emission tunability, emission spectra in the range 400–650 nm and for excitation in the range 295–425 nm were observed. The lifetime decay for polymer E was found to be 17.8 μs (Figure 1 f). The emission tunability can now be attributed to the formation of π-stacked pyrene units within polymer E. To support the growth of π-stacked energy states in polymer E being responsible for the emission tunability, theoretical analysis of the π-stacking was undertaken.

We performed quantum computations with the density functional approach by using the Gaussian 09[26] package for molecular-level understanding of the observed absorption phenomenon of our polymer E. It was previously reported that pyrene or pyrene derivatives show fluorescence owing to the formation of excimers.[27–30] Recently, it has also been reported that intermolecular photoinduced electron transfer (PET) and BET are also possible for pyrene, which causes intense fluorescence.[31] But, in all these cases, emission occurs in the blue region. At the same time, it is believed that the formation of excimers is not possible for polymer E. However, there are possibilities for electron transfer from the pyrene unit to any other unit. Similarly, it is expected in both the units that exist in our pyrene-based polymer film E. To test these possibilities, we computed absorption spectra of compounds formed from unit c (pyrene derivative) with unit b, unit c with unit a separately, and unit c with both unit a and unit b. The computed results are presented in Figure S25 (in the Supporting Information). We observe that all the lowest energy absorption peaks are located near 338 nm, which is where the lowest absorption peak of unit c is found. Thus, the emission of white light is not due to intramolecular charge transfer. There is only one possibility left that may be responsible for white light emission—π–π stacking of the π-electrons of pyrene rings, which exist in parallel orientation within the polymer film E. To test this possibility, we computed the absorption spectra of aggregated forms of unit c. We studied dimers, tetramers, and hexamers of unit c. A computed spectrum is presented in Figure 1 e. Absorption spectra of the pyrene derivative monomer, that is, unit c consists of three different peaks located at 338 nm, 266 nm, and 225 nm. Here, the lowest energy transition

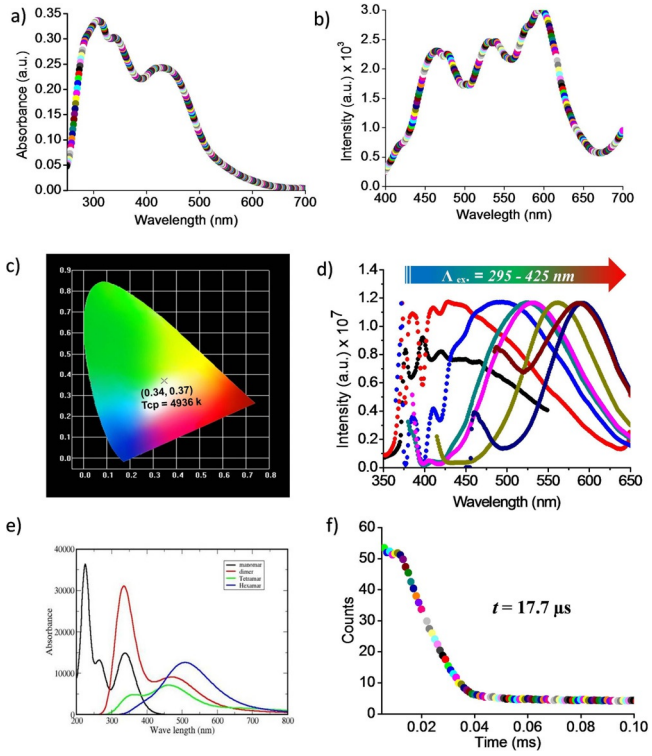

Figure 1. a) UV spectrum, b) fluorescence spectrum for excitation at 355 nm, c) CIE coordinate diagram, d) tunability of emission with switch in excitation energy, e) computed absorption spectra of aggregated pyrene derivative, and f) lifetime decay for the polymer E with lifetime of 17.7 µs.

(338 nm) occurs for the HOMO to LUMO electron transition. Both the HOMO and LUMO are located over the pyrene ring (Figure S26, in the Supporting Information). Thus, derivatization of pyrene does not contribute to the shift of the absorption spectra. Transitions corresponding to the other two peaks (266 nm and 225 nm) are dominated by HOMO−1 to LUMO and HOMO−1 to LUMO+2 electron transfers. All these MOs are also located on the pyrene ring (Figure S26, in the Supporting Information). Thus, the other peaks also do not undergo a change as a result of derivatization. Thus, the peaks shifted owing to aggregation. It is observed that with an increase of aggregation, the peaks merge into two peaks for the dimer and tetramer. This further reduces to one peak for the hexamer. In the hexamer, only one broad peak appears, which shows very good absorbance (more than 5000) in the visible region (400 nm to 650 nm). Thus, it could emit white light. To understand the redshift of spectra on aggregation, we studied key electron transitions of the hexamer. It is observed that the electron transition for the lowest energy absorption (710 nm), which is in the red colour zone, is dominated by the HOMO−1 to LUMO+6 transition. This is, in fact, the charge transfer from one pyrene ring to its nearest pyrene ring (Figure S27-Y1, in the Supporting Information). The key absorption in the green colour zone (542 nm) is dominated by the HOMO to LUMO+14 electron transfer. This transition is the charge transfer from the pyrene ring to the carbonyl π-electron (Figure S27-Y2, in the Supporting Information). Absorption in the blue colour zone (399 nm) is also due to pyrene ring electron transfer but it is quite complicated. Here, the π-electron cloud of two closest pyrene rings is simultaneously transferred to their nearest pyrene ring (Figure S27-Y3, in the Supporting Information). The important nature of these transitions is that they depend on aggregation and the compactness of aggregation.

With the theoretical analysis paralleling the spectroscopic observations, the aspect we looked for was the flexibility of polymer E. To analyse the material strength, polymer E was mounted onto the Universal Testing Machine (UTM). The respective length (*l*), breadth (*b*), and height (h) of the material were monitored ($l=7.01$ mm, $b=6.9$ mm, $h=3.09$ mm). The compression curve revealed the strength and elasticity of the film. The release of compressive pressure allowed the film to regain its usual form. The compression was performed over multiple cycles to analyse the elasticity. The polymer material tends to retain its linear elasticity over multiple cycles as shown in Figure 2. This promising property makes it as a potential model system for the development of organic photoluminescent materials that are easy to handle and can be applied to applications such as catalysis, OLEDs, etc.

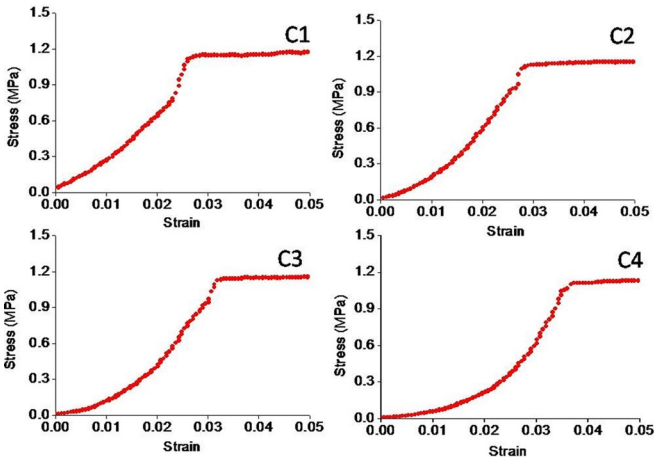

Figure 2. Compression analysis for the polymer film E over multiple cycles *Cn*.

Further, during our experimental fluorescence Mueller matrix measurements, we selected $\lambda=405$ nm beams and excited polymer E; this wavelength is close to the absorption band maxima at $\lambda=399$ nm. The fluorescence is found to be highly anisotropic both during excitation and emission. In this situation, polymer E likely undergoes a HOMO−1 to LUMO+27 transition with a negligible contribution from the HOMO to LUMO+14 and HOMO−1 to LUMO+6 transitions (see the Supporting Information for the anisotropic configuration obtained by using DFT calculations). This is the reason for the ground state (during excitation) anisotropy of the fluorescence, which is manifested as fluorescence diattenuation (differential excitation of fluorescence by orthogonal polarizations). We also saw higher anisotropy during emission of the fluorescence signal from polymer E, implying more organized emission of fluorescence from the excited state of the molecule manifesting as the fluorescence polarizance (differential emission of fluorescence with orthogonal linear polarization).

Experimental fluorescence Mueller matrix studies

A schematic representation of our home-built comprehensive experimental Mueller matrix fluorescence spectroscopy platform is introduced in Scheme 2d. The system is calibrated by using a robust Eigenvalue calibration method.[32,33] The specifics of the system and various steps of this method can be found elsewhere.[34] The recorded spectroscopic 4×4 fluorescence Mueller matrix (R) from polymer E is highlighted in Scheme 2d. Ground and excited state anisotropic information is extracted from the recorded R (λ).

Inverse analysis of fluorescence Mueller matrix for determination of molecular orientation

When light interacts with an optical medium, the output light is characterized by its Stoke vector $\boldsymbol{S}_{\mathbf{Out}} = R\boldsymbol{S}_{\mathbf{In}}$ in which $\boldsymbol{S}_{\mathbf{In}}$ and $\boldsymbol{S}_{\mathbf{Out}}$ are the input and output Stokes vectors, and R is the transfer function (Mueller matrix) of the medium, which contains all the polarization information of the system under study. There are several decomposition methods that may decouple the contributing polarization information from a recorded Mueller matrix. This polarization information has been successfully extracted by using several decomposition methods in case of elastic scattering. However, the existing decomposition methods are not valid for inelastic scattering processes such as fluorescence. Recent studies by our group and others have shown that for complex processes such as fluorescence the polarization information can be extracted from a recorded Mueller matrix as $R = M_{\Delta}M_{d}M_{0}$ in which M_{d} represents the depolarization effects that occur owing to the random orientation of the fluorophores and other extrinsic causes, M_0 and M_{Δ} represent the amplitude anisotropies of the ground and excited states of the fluorophore molecules (Figure S28, in the Supporting Information).[34] Finally, florescence anisotropy parameters can be obtained from the recorded fluorescence Mueller matrix (R) as [Eqs. (1) and (2)]:

$$\alpha_T = \frac{\sqrt{R_{12}^2 + R_{13}^2 + R_{14}^2}}{R_{11}}; \alpha_L = \frac{\sqrt{R_{12}^2 + R_{13}^2}}{R_{11}}; \alpha_C = \frac{R_{14}}{R_{11}}; \quad (1)$$

$$\beta_T = \frac{\sqrt{R_{21}^2 + R_{31}^2 + R_{41}^2}}{R_{11}}; \beta_L = \frac{\sqrt{R_{21}^2 + R_{31}^2}}{R_{11}}; \beta_C = \frac{R_{41}}{R_{11}}; \quad (2)$$

in which α_T, α_L, and α_C are the total, linear, and circular fluorescence diattenuation, respectively, and β_T, β_L, and β_C are the total, linear, and circular polarizance, respectively.

The anisotropy parameters contain information about the molecular orientation of the samples. Mueller matrix elements R_{13}/R_{12} and R_{31}/R_{21} represent the average fluorescent dipolar orientation angles for the ground (θ_{ex}) and the excited (θ_{em}) molecular states and can be expressed in terms of the recorded spectral Mueller matrix[35] as [Eq. (3)]:

$$\theta_{ex} = \frac{1}{2}\tan^{-1}\left(\frac{R_{13}}{R_{12}}\right); \theta_{em} = \frac{1}{2}\tan^{-1}\left(\frac{R_{31}}{R_{21}}\right) \quad (3)$$

Here, we define a molecular angular distribution function $f(\theta) = e^{-(\theta-\theta_{ex/em})^2}/2\Delta\theta_{ex/em}{}^2$ with width $\Delta\theta$ around the average fluorescent dipolar orientation angle (θ_{ex} and θ_{em}), which contains information about the distribution of the orientation angles of the molecules. Hence, the measured fluorescence intensity for excitation with a given polarization vector **E** can be written as [Eqs. (4) and (5)]:

$$I_\eta = \int_0^\pi \left|\mu \mathbf{E}_\eta\right|^2 f(\theta) d\theta = \quad (4)$$

$$(1-\eta)\int_0^\pi \cos^2(\theta) f(\theta) \mathrm{d}\theta + \eta \int_0^\pi \sin^2(\theta) f(\theta) \mathrm{d}\theta$$

$$\text{in which } \eta = \begin{cases} 0 \text{ for } H \\ 1 \text{ for } V \end{cases}$$

$$I_{P/M} = \int_0^\pi \left|\mu \mathbf{E}_{\frac{P}{M}}\right|^2 f(\theta) \mathrm{d}\theta \mu \int_0^\pi \cos^2\left(\theta \pm \frac{\pi}{4}\right) f(\theta) \mathrm{d}\theta \quad (5)$$

Figure 3a shows the recorded experimental normalized fluorescence Muller matrix. Figure 3b shows the extracted fluorescence linear (β_L) and circular (β_C) polarizance parameter and fluorescence linear (α_L) and circular (α_L) diattenuation using Equation (1). Figure 3c shows the wavelength variation of the average fluorescent dipolar orientation angles for the ground (θ_{ex}, blue dashed line) and the excited (θ_{em}, red solid line) molecular states using Equation (2). Figure 3d shows the derived molecular angular distribution function for the ground ($f_{ex}(\theta)$, blue solid line) θ_{ex} and the excited ($f_{ex}(\theta)$, red dashed line) molecular states of the fluorescent molecule. Several interesting trends can be obtained from these figures. The first element (R_{11}) of the recorded experimental normalized fluorescence Muller matrix represents the total fluorescence intensity. The elements in the first row coloured in blue represent the intrinsic anisotropic properties of the ground molecular states. Similarly, elements in first column of the MM highlighted in red represent the emission state anisotropy of the molecules in the excited state. The diagonal elements of MM are related to the depolarization effects associated with the fluorescence process. Elements R_{23}, R_{24}, R_{34}, R_{32}, R_{42}, and R_{43} are related to the phase anisotropy effect associated with the fluorescence process, which is negligible (close to zero) in case of fluorescence scattering. In Figure 3b, we show the linear and circular anisotropy of the polymer E. The linear anisotropy of the excited molecular state is higher than that of the ground molecular state, which means the excited molecular state is more organized than the ground molecular state. However, the circular anisotropy has a negligible value, implying that the molecules possess no chirality, which is also confirmed by the DFT simulation. The ground and excited state molecular orientation angles are plotted in Figure 3c. We have plotted the distribution function to understand the molecular orientation. As the excited molecular state anisotropy parameter (β_L) is significantly larger compared with the ground state anisotropy parameter (α_L), the excited molecular states are more organized than the ground states, accordingly the standard deviation $\Delta\theta_{ex}$ is larger than $\Delta\theta_{em}$. The molecular distribution functions $f_{ex}(\theta)$

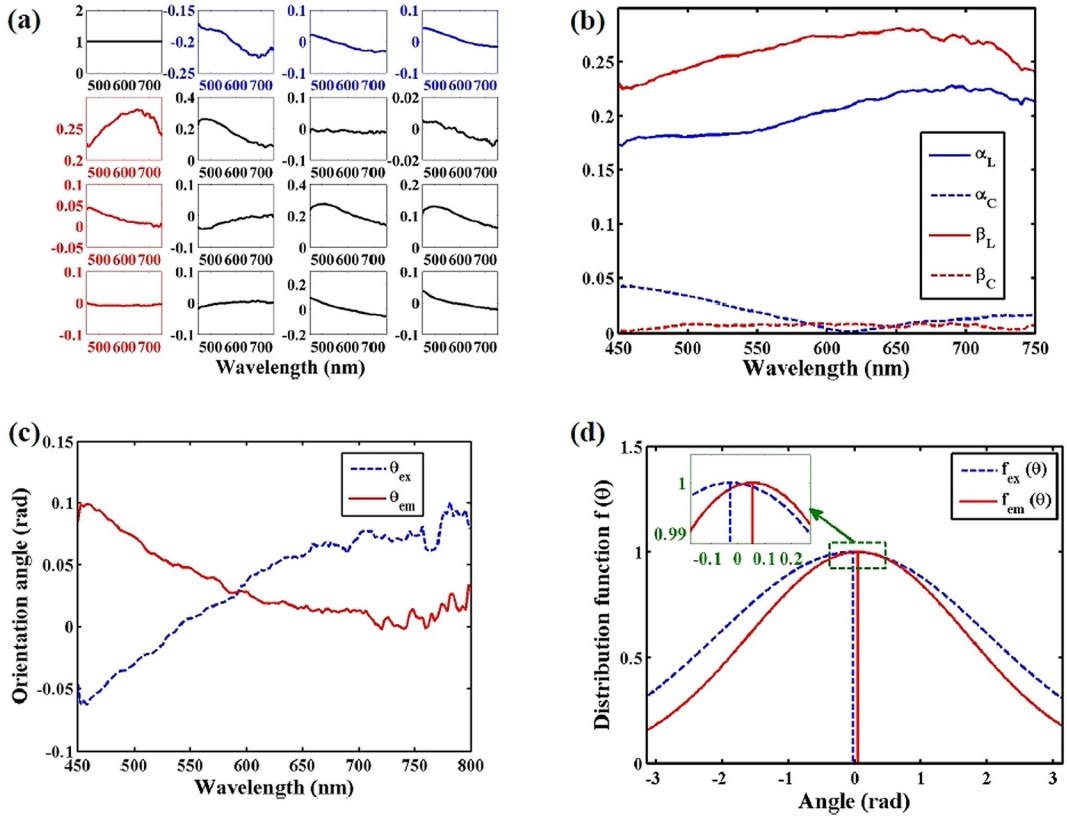

Figure 3. a) Normalized fluorescence spectroscopic Mueller matrix. b) The fluorescence diattenuation and polarizance parameters. c) Wavelength variation of the average fluorescent dipolar orientation angles for the ground (θ_{ex}, blue dashed line) and the excited (θ_{ex}, solid red line) molecular states. d) The derived molecular angular distribution function for the ground ($f_{ex}(\theta)$, blue dashed line) θ_{ex} and the excited ($f_{em}(\theta)$, solid red line) molecular states of the fluorescent molecule. Inverse calculations were performed on the Mueller matrix-derived α_L and β_L parameters to extract this information. The estimated standard deviations of the orientation angle distribution for the ground and excited states were found to be $\Delta\theta_{ex} = 0.02614$ rad and $\Delta\theta_{em} = 0.05397$ rad, respectively. The vertical lines mark the centre positions of the distribution functions.

and $f_{em}(\theta)$ were calculated near the peak of the fluorescence intensity (520 nm). Note that π–π stacking of pyrene moieties and the thiol–alkene photoclick radical polymerization reaction of the norbornene monomers generated a single one-product material within the crosslinked framework. This leads to preferential linear organization of the fluorescent molecular dipoles (of pyrene units), which appears to be the underlying reason for the considerably high magnitudes of the fluorescence anisotropy, α_L and β_L parameters.

Polarization controlled tuning of fluorescence spectra

The strong polarization anisotropy of fluorescence of the crosslinked polymer E provides a useful handle to control the emitted spectral intensity of the fluorescence by using a proper pre- and post-selection of the set of polarization states. To get the much desired control over the emitted fluorescence intensity without changing the physical or chemical properties of the polymer E, we have used a general approach using polarization state projection on the recorded fluorescence Mueller matrix ($I(\lambda) = 1/2\boldsymbol{S}_{out}^{T} M(\lambda)\boldsymbol{S}_{in}$). The fluorescence intensity can be desirably enhanced or suppressed by orders of magnitude by using different pre- and post-selected polarization states, as illustrated in Figure 4. This also leads to systematic changes in the spectral line shape of the emission (shown in the inset, where the area normalized spectral line shapes are displayed).

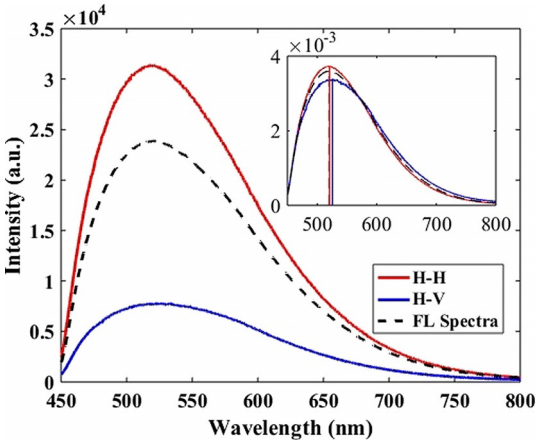

Figure 4. Comparison of polarization projected intensity using different pre- and post-selected states: the polarization independent fluorescence spectra is shown by the black dashed line, the recorded fluorescence intensity for input horizontal pre-selection and horizontal (vertical) post-selection state is shown by the red (blue) solid curve. The inset shows spectral variations of area normalized to the projected intensities of the same. The vertical line in each curve corresponds to the maximum position of the corresponding intensity.

The emitted fluorescence spectra with horizontal input and detection with horizontal and vertical post-selection are shown by the red and solid blue curves, respectively. By using horizontal pre- and post-selection, the emitted fluorescence signal is observed to be considerably enhanced for unpolarized fluorescence intensity, which is accompanied by subtle changes in the line shape. For detection with vertical post-selection for horizontal pre-selection leads to more apparent shifts in the peak position ($\approx$5 nm) and a more drastic reduction in the intensity of emission. The fluorescence anisotropy properties, namely, linear fluorescence diattenuation (differential excitation of fluorescence by orthogonal linear polarizations) and the fluorescence polarizance (differential emission of fluorescence with orthogonal linear polarization) properties of the OLED sample are responsible for such differential spectral intensity profiles for different linear polarizations. Thus, in these intrinsically anisotropic systems, pre- and post-selection of the polarization states provides a unique handle to desirably control both the intensity and the spectral line shape of emission without changing the chemical composition or molecular organization of the sample. This remarkable feature of polymer E may find useful application for developing polarization controlled tunable devices for diagnostics and imaging, apollo sensors, and logic gates.[36–38]

Conclusions

In this article, we have successfully demonstrated the emission properties of the newly synthesized photoluminescent 3D polymer film E, which covers a wide RGB range from spectroscopic analysis. This synthesized polymer E exhibits physical properties such as flexibility and mechanical strength in relation to compressibility, which could be useful as an efficient organic spin-optical device.

Moreover, the theoretical analysis confirms π–π stacking leads to formation of dimers, trimers, tetramers, pentamers, and so on, which covers the region of our interest. Also, we have quantified the excited and emission state anisotropies arising from the orientation and organization of organic polymer film E through the fluorescence diattenuation and fluorescence polarizance parameters. These parameters are further used to quantify the molecular orientational order of the organic LED sample. Finally, the information contained in the fluorescence Mueller matrix is exploited for polarization-controlled tuning of spectral intensity of emission. Thus, the modelled organic polymer E holds considerable promise and could turn out to be a potential candidate for devices related to catalysis, sensing, diagnostics and imaging, light emission as OLEDs, etc. In particular, the polarization-controlled tuning of the intensity may also have useful applications in this domain.

Acknowledgments

R.K. thanks DBT for a research fellowship. S.M. and S.R. thank CSIR and UGC for research fellowships. S.S. and A.B. thank IISER Kolkata for fellowships. R.S. thanks DBT and DST-SERB for research projects. The authors thank IISER-Kolkata for the infrastructure facilities.

Conflict of interest

The authors declare no conflict of interest.

Keywords: anisotropy · density functional calculations · photoluminescence · pi–pi interactions · polarization

[1] A. Tsuboyama, H. Iwawaki, M. Furugori, T. Mukaide, J. Kamatani, S. Igawa, T. Moriyama, S. Miura, T. Takiguchi, S. Okada, M. Hoshino, K. Ueno, *J. Am. Chem. Soc.* **2003**, *125*, 12971 – 12979.
[2] P. L. dos Santos, J. S. Ward, M. R. Bryce, A. P. Monkman, *J. Phys. Chem. Lett.* **2016**, *7*, 3341 – 3346.
[3] R. M. Chalke, V. R. Patil, *Polymer* **2017**, *123*, 355 – 365.
[4] K. B. Ivaniuk, G. V. Baryshnikov, P. Y. Stakhira, S. K. Pedersen, M. Pittelkow, A. Lazauskas, D. Volyniuk, J. V. Grazulevicius, B. F. Minaev, H. Agren, *J. Mater. Chem. C* **2017**, *5*, 4123 – 4128.
[5] F. Xu, K. W. Hershey, R. J. Holmes, T. R. Hoye, *J. Am. Chem. Soc.* **2016**, *138*, 12739 – 12742.
[6] B. A. Ikkanda, B. L. Iverson, *Chem. Commun.* **2016**, *52*, 7752 – 7759.
[7] E. Gautier-Thianche, C. Sentein, A. Lorin, J.-M. Nunzi, *Opt. Mater.* **1999**, *12*, 295 – 299.
[8] Z. Bao, J. A. Rogers, A. Dodabalapur, A. J. Lovinger, H. E. Katz, V. R. Raju, Z. Peng, M. E. Galvin, *Opt. Mater.* **1999**, *12*, 177 – 182.
[9] Q. Pei, Y. Yang, G. Yu, C. Zhang, A. J. Heeger, *J. Am. Chem. Soc.* **1996**, *118*, 3922 – 3929.
[10] P. Zalar, D. Kamkar, R. Naik, Ouchen, J. G. Grote, G. C. Bazan, T-Q. Nguyen, *J. Am. Chem. Soc.* **2011**, *133*, 11010 – 11013.
[11] S. Tang, J. Pan, H. A. Buchholz, L. Edman, *J. Am. Chem. Soc.* **2013**, *135*, 3647 – 3652.
[12] H. C. Kolb, M. G. Finn, K. B. Sharpless, *Angew. Chem. Int. Ed.* **2001**, *40*, 2004 – 2021; *Angew. Chem.* **2001**, *113*, 2056 – 2075.
[13] W. Tang, M. L. Becker, *Chem. Soc. Rev.* **2014**, *43*, 7013 – 7039.
[14] R. Kumar, R. Shunmugam, *ACS Omega* **2017**, *2*, 4100 – 4107.
[15] C. E. Hoyle, C. N. Bowman, *Angew. Chem. Int. Ed.* **2010**, *49*, 1540 – 1573; *Angew. Chem.* **2010**, *122*, 1584 – 1617.
[16] J. R. Lakowicz, *Principles of Fluorescence Spectroscopy*, Springer US, New York, **1983**.
[17] N. Ghosh, I. A. Vitkin, *J. Biomed. Opt.* **2011**, *16*, 110801 – 110829.
[18] D. H. Goldstein, *Polarized Light*, CRC, Boca Raton, **2016**.
[19] O. Arteaga, S. Nichols, B. Kahr, *Opt. Lett.* **2012**, *37*, 2835 – 2837.
[20] S. Satapathi, J. Soni, N. Ghosh, *Appl. Phys. Lett.* **2014**, *104*, 131902.
[21] S. Saha, J. Soni, S. Chandel, U. Kumar, N. Ghosh, *J. Biomed. Opt.* **2015**, *20*, 085005.
[22] K.-C. Tang, M.-J. Chang, T.-Y. Lin, H.-A. Pan, T.-C. Fang, K.-Y. Chen, W.-Y. Hung, Y.-H. Hsu, P.-T. Chou, *J. Am. Chem. Soc.* **2011**, *133*, 17738 – 17745.
[23] H. Namai, H. Ikeda, Y. Hoshi, N. Kato, Y. Morishita, K. Mizuno, *J. Am. Chem. Soc.* **2007**, *129*, 9032 – 9036.
[24] C. Hazra, V. N. K. B. Adusumali, V. Mahalingam, *ACS Appl. Mater. Interfaces* **2014**, *6*, 7833 – 7839.
[25] V. N. K B. Adusumali, H. V. S. R. M. Koppiesetti, V. Mahalingam, *J. Mater. Chem. C* **2016**, *4*, 2289 – 2294.
[26] Gaussian 09, Revision D.01, M. J. Frisch, G. W. Trucks, H. B. Schlegel, G. E. Scuseria, M. A. Robb, J. R. Cheeseman, G. Scalmani, V. Barone, B. Mennucci, G. A. Petersson, H. Nakatsuji, M. Caricato, X. Li, H. P. Hratchian, A. F. Izmaylov, J. Bloino, G. Zheng, J. L. Sonnenberg, M. Hada, M. Ehara, K. Toyota, R. Fukuda, J. Hasegawa, M. Ishida, T. Nakajima, Y. Honda, O. Kitao, H. Nakai, T. Vreven, J. A. Montgomery, Jr., J. E. Peralta, F. Ogliaro, M. Bearpark, J. J. Heyd, E. Brothers, K. N. Kudin, V. N. Staroverov, R. Kobayashi, J. Normand, K. Raghavachari, A. Rendell, J. C. Burant, S. S. Iyengar, J. Tomasi, M. Cossi, N. Rega, J. M. Millam, M. Klene, J. E. Knox, J. B. Cross, V. Bakken, C. Adamo, J. Jaramillo, R. Gomperts, R. E. Stratmann, O. Yazyev, A. J. Austin, R. Cammi, C. Pomelli, J. W. Ochterski, R. L. Martin, K. Morokuma, V. G. Zakrzewski, G. A. Voth, P. Salvador, J. J. Dannenberg,

S. Dapprich, A. D. Daniels, O. Farkas, J. B. Foresman, J. V. Ortiz, J. Cioslowski, D. J. Fox, Gaussian, Inc., Wallingford CT, **2009**.
[27] S. K. Kim, J. H. Bok, R. A. Bartsch, J. Y. Lee, J. S. Kim, *Org. Lett.* **2005**, *7*, 4839 – 4842.
[28] J. Huang, Y. Wu, Y. Chen, Z. Zhu, X. Yang, C. J. Yang, K. Wang, W. Tan, *Angew. Chem. Int. Ed.* **2011**, *50*, 401 – 404; *Angew. Chem.* **2011**, *123*, 421 – 424.
[29] J. B. Birks, L. G. Christophorou, *Spectrochimica Acta* **1963**, *19*, 401 – 410.
[30] P. Conlon, C. J. Yang, Y. Wu, Y. Chen, K. Martinez, Y. Kim, N. Stevens, A. A. Marti, S. Jockusch, N. J. Turro, W. Tan, *J. Am. Chem. Soc.* **2008**, *130*, 336 – 342.
[31] S. Narra, Y. Nishimura, H. A. Witek, S. Shigeto, *ChemPhysChem* **2014**, *15*, 2945 – 2950.
[32] E. Compain, S. Poirier, B. Drevillon, *Appl. Opt.* **1999**, *38*, 3490 – 3502.
[33] J. Soni, H. Purwar, H. Lakhotia, S. Chandel, C. Banerjee, U. Kumar, N. Ghosh, *Opt. Express* **2013**, *21*, 15475 – 15489.
[34] R. M. A. Azzam, *J. Opt. Soc. Am.* **1978**, *68*, 1756 – 1767.
[35] K. Maji, S. Saha, R. Dey, N. Ghosh, D. Haldar, *J. Phys. Chem. C* **2017**, *121*, 19519 – 19529.
[36] S. J. Jameson, J. A. Ross, *Chem. Rev.* **2010**, *110*, 2685 – 2708.
[37] W. D. Cameron, C. V. Bui, A. Hutchinson, P. Loppanau, S. Graslund, J. V. Rocheleau, *Nat. Methods* **2016**, *13*, 352 – 358.
[38] Y. Yang, K. Z. Wang, D. Yan, *ACS Appl. Mater. Interfaces* **2017**, *9*, 17399 – 17407.

Manuscript received: May 21, 2019
Revised manuscript received: July 22, 2019
Accepted manuscript online: August 1, 2019
Version of record online: September 13, 2019